Experimental and numerical investigation of 3D aerofoil characteristics on a MW wind turbine

Troldborg, Niels; Bak, Christian; Sørensen, Niels N.; Aagaard Madsen , Helge; Réthoré, Pierre-Elouan; Zahle, Frederik; Guntur, Srinivas

Published in:
Proceedings - European Wind Energy Conference & Exhibition 2013

Publication date:
2013

Experimental and numerical investigation of 3D aerofoil characteristics on a MW wind turbine

Niels Troldborg* Christian Bak* Niels N. Sørensen* Helge A. Madsen* Pierre-Elouan Réthoré* Frederik Zahle* Srinivas Guntur*
*Wind Energy Department, Risø campus, DTU, DK-4000 Roskilde, Denmark
niet@risoe.dtu.dk

Abstract

3D aerofoil characteristics on a MW wind turbine is investigated through a combination of field measurements, wind tunnel tests and computational fluid dynamics (CFD). Surface pressure measurements as well as the integrated force coefficients for selected aerofoil sections on a blade of the turbine is compared to wind tunnel measurements on the same aerofoil sections in order to reveal the difference in performance of aerofoils on full scale rotors in atmospheric conditions and aerofoils in wind tunnels. The findings of the measurements are backed up by analogous CFD analysis involving fully resolved 3D computations on the wind turbine as well as 2D aerofoil simulations.
Keywords: Rotor aerodynamics, aerofoil aerodynamics, full scale measurements, wind tunnel measurements, Rotor CFD, Aerofoil CFD

1 Introduction

Aerodynamic aerofoil characteristics used for design of wind turbines are usually obtained from 2D wind tunnel tests. However, the actual 3D aerofoil characteristics on a rotor can be quite different from those measured in a wind tunnel because of centrifugal forces in the boundary layer, spanwise pressure gradients generated by the Coriolis force as well as unsteady and turbulent inflow conditions. In effect a direct application of the 2D characteristics shows bad agreement between measured and calculated loads especially at the inner part of the blade where the 3D effects are most dominant. A number of empirical models have been proposed to derive 3D data from 2D data [3, 6, 7, 9, 12, 23]. These models usually takes into account the effect of centrifugal and Coriolis forces. Even though some of these models can improve predictions of thrust and power there are still a big difference between measured and corrected aerofoil characteristics at high angles attack. In order to improve new and existing models more fundamental knowledge is needed about the nature of 3D aerofoil flows on a wind turbine.

One way to gain more insight into 3D aerofoil characteristics is from full 3D rotor computations using Computational Fluid Dynamics (CFD), which benefits from providing all details about the flow field. However, when using CFD there are also important uncertainties due to inadequate turbulence and transition modelling but also because these simulations are usually restricted to non-turbulent, steady inflow conditions. Therefore, typical full rotor CFD cannot stand alone when investigating aerofoil characteristics on a wind turbine.

Aerodynamic loads on wind turbine rotors have also been studied through a number of field test measurements [2, 15]. These investigations improved the insight into 3D aerofoil characteristics on rotors considerably. However, it was also realized that the influence of the natural turbulence in the wind complicated the interpretation of the results. This limitation was overcome in the NREL Unsteady Aerodynamics Experiment [10] and the MEXICO project [22] in which comprehensive measurements were carried out on wind turbines in large wind tunnels. The above mentioned data sets have contributed significantly to model development and validation and not the least for validation of CFD rotor computations. On the other hand there are some serious limitations for the wind tunnel models when knowledge should be transferred to full scale MW rotors. The most important is the influence from the unsteady and turbulent inflow, which in the end has to be taken into account although it complicates detailed aerodynamic measurements as well as simulations. Another major drawback of the wind tunnel data sets is that the rotors are not representative for modern MW rotor designs. Finally, there is always the uncertainty from the much lower Reynolds number in the wind tunnel experiments compared with full-scale conditions. Thus, the derivation of aerofoil characteristics still introduces uncertainties in the rotor design process.

That was the reasons for setting up the DANAERO MW tests, where both the aerodynamics and loads can be studied in detail on a 2MW NM80 wind turbine [4, 5, 13, 14]. In addition to the field experiment on the NM80 turbine, measurements of four aerofoil sections were conducted in the LM Wind Power wind tunnel. The four aerofoil sections had a shape nearly identical to different cross-sections of the LM38.8 blade of the NM80 turbine. In this way the DANAERO experiment provides a unique dataset for looking into the difference of aerofoil characteristics obtained in a wind tunnel and under atmospheric flow conditions.

However, in appreciation of the limitations of both measurements and computations we will in the present paper be utilizing both 2D aerofoil CFD, full 3D rotor CFD as well as the wind tunnel and field measurements from the DANAERO experiment to study 3D aerofoil characteristics in comparison with aerofoil performance in 2D flow.

2 Experimental approach

Two different types of measurements obtained within the DANAERO experiment are used as a basis for the present work:

1) Pressure and inflow measurements on one of the LM38.8 blades on the NM80 2 MW turbine at the small Tjæreborg Wind farm in Denmark. Surface pressure distributions were measured at the four radial stations, r/R=0.325, 0.475, 0.750 and 0.925 where the relative thickness of the aerofoils was 33%, 24%, 20% and 19%, respectively. Each of the four sections were instrumented with 64 pressure taps. Inflow measurements were provided from a met mast located nearby and from four five-hole Pitot tubes mounted at r/R=0.36, 0.51, 0.78 and 0.90, respectively.

2) 2D wind tunnel measurements on four aerofoils with nearly the same geometry as the four blade sections on the LM38.8 blade which were instrumented with pressure taps.

These data creates a basis for studying how the aerodynamic characteristics on a real wind turbine deviates from those obtained in 2D in a wind tunnel.

3 Computational approach

Two different types of simulations are carried out using the in-house incompressible finite volume Reynolds Averaged Navier-Stokes (RANS) flow solver EllipSys [19, 20, 25]:

1) 2D steady state simulations on the four aerofoil sections using the $k-\omega$ SST turbulence model [16] and a correlation based transition model [17, 18, 24].The grids used for the simulations were of the O-mesh type. The domain height was set to approximately 30 chord lengths and the height of the first cell adjacent to surface was set to 10^{-6} chord lengths corresponding to a maximum y^+ of approximately 0.2. All grids had 256 cells around the aerofoil and 128 cells normal to the aerofoil.

2) 3D rotor computations on the NM80 turbine in steady and uniform inflow using the same turbulence and transition models as used for the 2D simulations. In the simulations the rotor geometry and the blade surface boundary layer is fully resolved using a standard O-O mesh configuration. The radius of the domain was approximately 10 rotor diameters and the height of the first cell adjacent to the blade surface was set to satisfy the condition $y^+ < 1$ as required for this type of computations. The blades of the turbines were resolved with $256 \times 128 \times 128$ cells in the chordwise, spanwise and normal direction, respectively. The grid consisted of 432 block of 32^3 $(14 \cdot 10^6)$ grid cells.

These computed data can be considered analogous to the experimental datasets and forms a basis for studying the difference between 2D and 3D aerofoil characteristics.

4 Results

In the following selected results from the analysis of measurements and simulations will be presented.

4.1 Comparison of wind tunnel measurements and 2D simulations

In this section the wind tunnel measurements and 2D aerofoil computations are validated by comparing them against each other.

Figure 1 shows C_p distributions at three different angles of attack (AoA) for smooth aerofoils at a Reynolds number of $Re = 5 \cdot 10^6$. For the sections at r/R=0.475, 0.750 and 0.925 the agreement is good except at the highest AoA, where the computations predicts a much larger suction peak than observed in the measurements. Similar discrepancies have been seen in previous work [8] and indeed these aerofoils are quite challenging to simulate at high AoA because the transition point is located rather far aft on these aerofoils. For the thickest aerofoil (r/R=0.325) there are quite large discrepancies between computations and measurements for all AoA. The reason for these

discrepancies are most likely due to tunnel blockage and 3D effects caused by the walls of the wind tunnel. While 3D effects are also present for thin aerofoils they are only important at higher AoA. As shown in [1] 3D effects are particularly pronounced for thick aerofoils as well as at high AoA and in order to predict the correct stalling behaviour the inclusion of the tunnel walls is important as these may play an important role in the actual aerodynamic behaviour of the aerofoil in the wind tunnel.
Figures 2-3 shows C_L and C_D polars for each section. The lift and drag coefficients are defined as:

$$C_L = \frac{F_L}{\frac{1}{2}\rho c V_{rel}^2}$$
$$C_D = \frac{F_D}{\frac{1}{2}\rho c V_{rel}^2}$$

where F_L and F_D is the lift and drag force per meter, respectively, ρ is the air density, V_{rel} is the relative velocity and c is the local chord length.
Computations have been carried out assuming both transitional and fully turbulent flow over the aerofoil surface. For the three thinnest sections the computed $C_{L,max}$ is significantly higher than the measured, which is as expected from the C_p distributions shown in Figure 1. For the thickest aerofoil the computed and measured lift coefficient does not show much resemblance, which is most likely a combined consequence of wind tunnel effects and the inadequacy of simulating the flow over thick aerofoils as 2D. In all cases the simulations are seen to predict higher drag at low AoA than what is measured in the wind tunnel. This is because the used grid resolution in the chordwise direction is not sufficiently high for this type of aerofoils. We did simulations with increased chordwise resolution of 384 cells and found that the drag in these simulations were in much closer agreement with measurement at low AoA. However, these results are not shown here because we want to make a one-to-one comparison with the 3D computations where 256 grid cells were used in the chordwise direction.

4.2 Comparison of field measurements and 3D rotor simulations

In order to validate the 3D rotor computations and the field measurements a comparison of the pressure distributions along the four investigated blade sections was conducted at different operational conditions.
For the comparison 1-minute averages of C_p distributions were extracted from the DANAERO database in cases where the turbine was operating in undisturbed flow at nearly constant rotational speed and pitch. During the DANAERO field measurement campaign a number of tests were carried out where the turbine was forced to operate at fixed pitch and rotational speed. Even though this means that the turbine is operating off design in these cases they are suitable for comparison with CFD. In all cases the measured C_p distribution is computed as:

$$C_p = \frac{p - p_\infty}{\frac{1}{2}\rho\left(V_\infty^2 + (r\Omega)^2\right)}$$

where V_∞ is the free-stream velocity measured by the met mast located nearby, P_∞ is the ambient pressure, r is the radial position of the blade section, Ω is the rotational speed of the turbine and ρ is the air density.
Figures 4-5 compare measured and computed pressure distributions at different free-stream velocity and operational conditions as specified in the figure captions. Note that a negative pitch angle means towards stall. The errorbars included in the plots shows the standard deviation of the measured 1 minute averages and thus represent the scatter in the measurements. As seen the pressure distributions are generally in quite good agreement and the numerical predictions generally lie within the uncertainty bars. However, a general trend is that the computed suction peak for the two outermost sections is over predicted in comparison with measurements. The discrepancies may be explained as differences in inflow conditions caused by wind shear/veer, turbulence and yaw error.

4.3 Comparison of 2D and 3D aerofoil characteristics

In order to compare 2D and 3D aerofoil characteristics it is necessary to determine the angle of attack (AoA) at the different blade sections on the rotor blade. Several methods have been proposed for this purpose. Here we use the azimuthal averaging technique (AAT) employed by Hansen and Johansen [11, 21] in which the velocity, at a given radial position in the rotor plane, is calculated using the azimuthally averaged velocity at axial positions up and downstream of the rotor. Since the AAT requires information about the velocity field both up and downstream we can not use it to estimate the AoA from the measurements. Instead the AoA in the measurements is computed using the following procedure:

- Extract measured 1-minute averaged C_p^{exp} distributions for each blade section and bin average them on the flow angle measured directly by

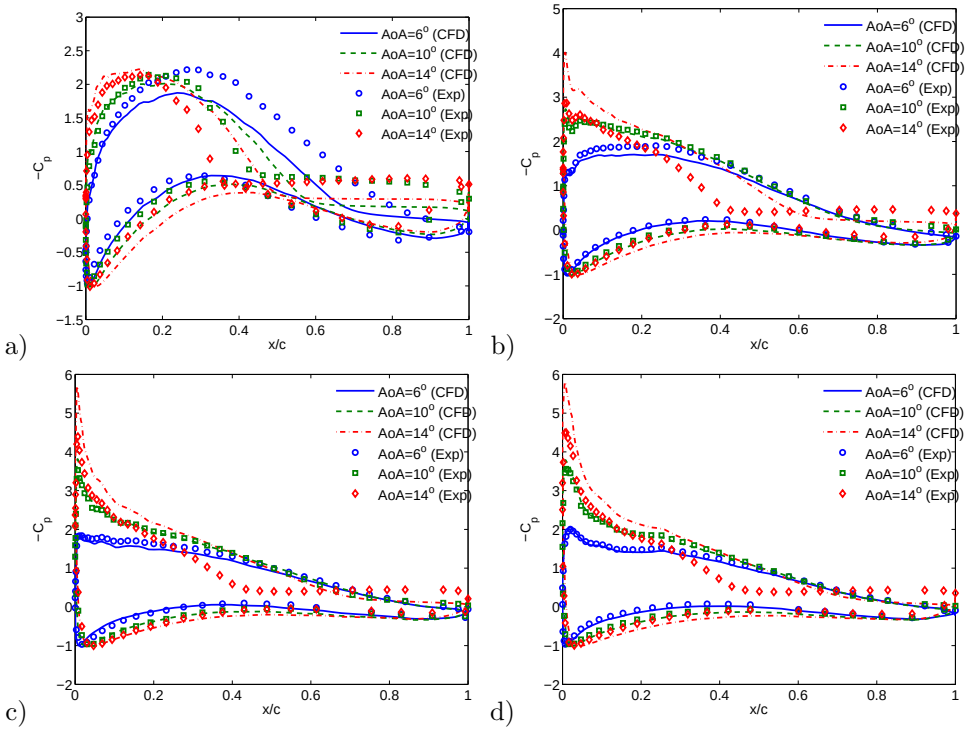

Figure 1: *C_p^* distributions predicted from wind tunnel measurements and 2D computations.a) r/R=0.325; b) r/R=0.475; c) r/R=0.750; d) r/R=0.925.*

the pitot tube located at r/R=0.78 using bins of $\pm 0.5^o$, i.e. establish $C_p^{exp}(AoA_{pitot})$

- From the 3D rotor computations determine the AoA for each blade section using the AAT and establish the computed $C_p^{cfd}(AoA)$.
- Estimate the measured AoA in an optimization process involving minimizing the objective function:

$$min \left\| \sum_{i=1}^{n} \left(C_p^{exp}(AoA_{pitot}) - C_p^{cfd}(AoA) \right)^2 \right\|$$

where $n = 64$ is the number of pressure taps along the aerofoil section.

In this way transfer functions from AoA_{pitot} to AoA in 3D is established.

Figures 6-7 show measured and computed C_p distributions at the different blade sections in comparison with the corresponding distributions obtained in the wind tunnel and using 2D computations. Generally, the agreement between the measurements on the rotor and the rotor computations is fairly good. The observed discrepancies is partly due to uncertainties in determining C_p from the measurements where we do not know the true free-stream velocity but also due to inadequate turbulence modelling.

For $AoA = 6^o$ the flow appears to be 2D over most of the blade span but even at this low AoA there are important difference between 2D and 3D flows at the inner and outermost sections. The pressure over the suction side is generally slightly higher in 2D than in 3D. We cannot explain this difference but it is interesting to notice that it appears both in the computations and in the measurements.

At the high AoAs, the suction over most of the upper aerofoil surface at r/R=0.325 is higher in 3D than in 2D and also the position where a nearly constant pressure level is reached is closer to the trailing edge in 3D than in 2D. This indicates a delay in stall on the rotor compared to the 2D case. This stall delay can be explained to be caused by the presence of Centrifugal/Coriolis on the rotor.

Figure 8-9 shows respectively the normal and tangential force coefficients integrated from the pressure distributions. The normal force coefficient, C_n, and the tangential force coefficient, C_t, are defined as:

$$C_n = \frac{F_n}{\frac{1}{2}\rho c \left(V_\infty^2 + (r\Omega)^2\right)}$$

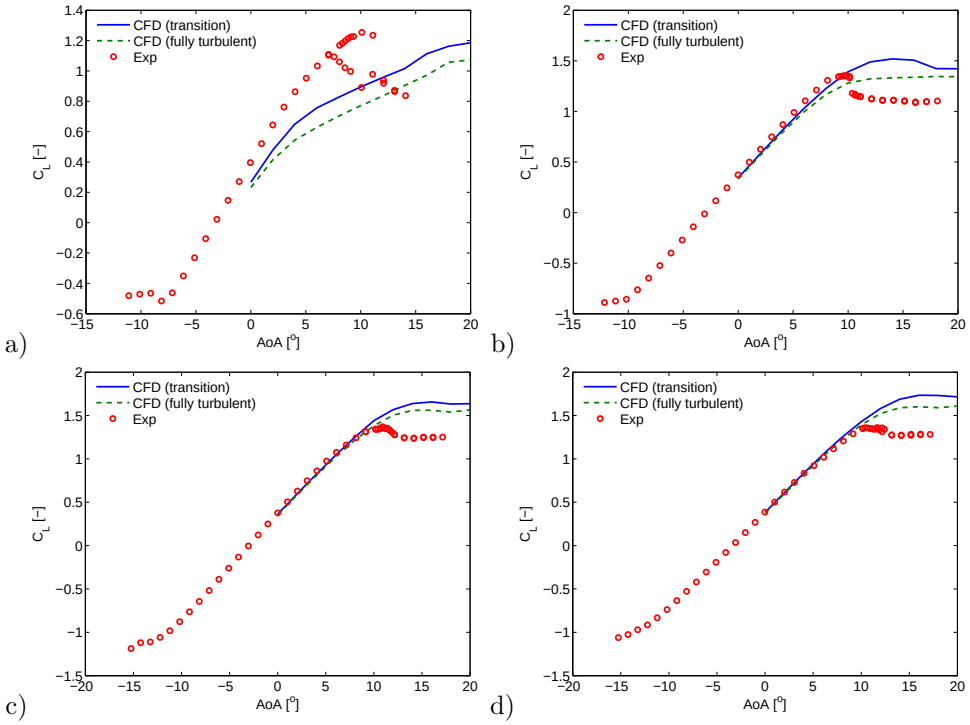

Figure 2: *Lift coefficient predicted from wind tunnel measurements and 2D aerofoil computations. a) r/R=0.325; b) r/R=0.475; c) r/R=0.750; d) r/R=0.925.*

$$C_t = \frac{F_t}{\frac{1}{2}\rho c\left(V_\infty^2 + (r\Omega)^2\right)}$$

where F_n and F_t is the normal and tangential force per meter, respectively, integrated from the C_p distributions.

Generally, the agreement between 3D rotor computations and rotor measurements is good, however there are important differences at r/R=0.750, where it seems that C_n measured on the rotor is closer to the $2D$ computations.

At high AoA the C_n values indicate delay in stall at r/R=0.325 and r/R=0.475. At the outermost section the C_n values are below the 2D values for all AoA and it also seems that the slope of the C_n curve is lower in 3D than in 2D. Shen et al. [26] showed similar behaviour of the lift coefficient near the tip of a rotor. From Figure 7 it appears that the lower C_n is caused by a reduction in the suction peak.

5 Conclusion

The aerodynamic performance of aerofoils on a MW wind turbine is investigated and compared to the corresponding aerofoil characteristics deduced in a wind tunnel and as predicted from both 2D aerofoil simulations and full 3D rotor computations using CFD. The combination of field tests, wind tunnel measurements as well as 2D and 3D CFD provides a unique dataset for studying the complex phenomena of 3D aerofoil characteristics.

Initially wind tunnel measurements on four different aerofoil sections were compared to 2D aerofoil simulations. The agreement was found to be fairly good but there were important differences at high angles of attack (AoA). For the thickest aerofoil large difference was found between measured and computed aerofoil performance. These difference was argued to be partly due to wall effect in the tunnel but also because it may be inadequate to simulate thick aerofoils at high AoA using 2D CFD.

Secondly a comparison of surface pressure distributions predicted from full rotor CFD and measurements showed rather good agreement at both low and high inflow velocities.

Finally, a comparison of 2D and 3D aerofoil performance was conducted. It was shown that the aerofoil at the inner section (r/R=0.325) experienced augmented performance compared to 2D because of centrifugal and Coriolis forces. For the outermost section (r/R=0.925) it was found that both the overall

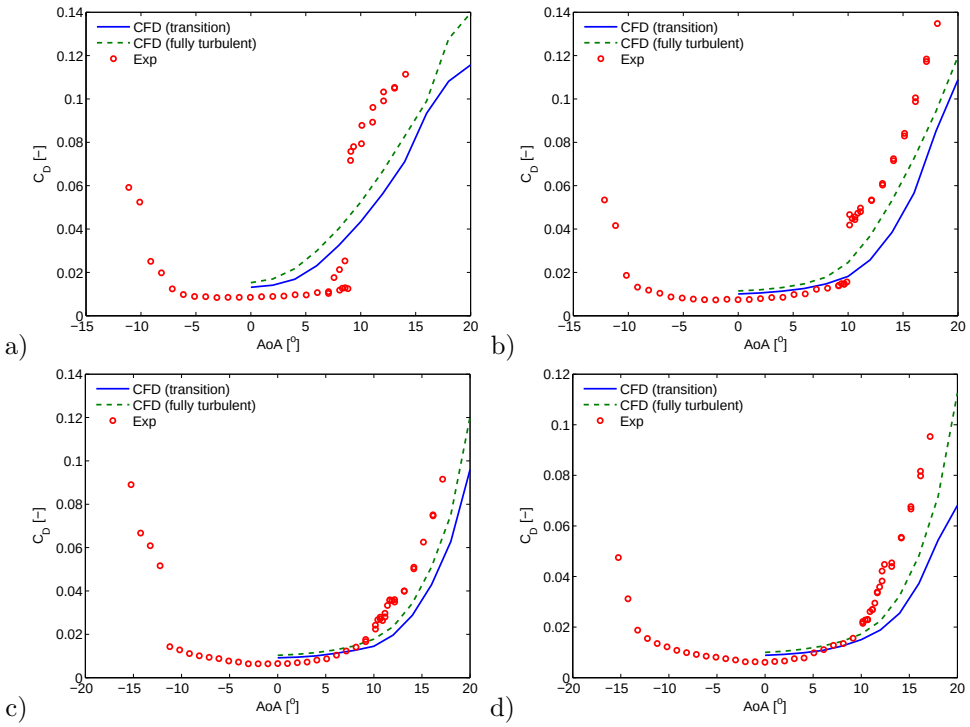

Figure 3: *Drag coefficient predicted from wind tunnel measurements and 2D aerofoil computations. a) r/R=0.325; b) r/R=0.475; c) r/R=0.750; d) r/R=0.925.*

level and the slope of the normal force coefficient (C_n) curve was lower than in 2D. For the mid span sections the aerofoil characteristics was found to be rather 2D.

Acknowledgement

This work has been funded by the EUDP WTopt project (no 64011-0346), the Danish Strategic Research Council (DSF) within the project *Center for Computational Wind Turbine Aerodynamics and Atmospheric Turbulence* (no 2104-09-0026), the Danish Energy Authorities, EFP2007 and EUDP2009-II as well as by the different project partners. Thanks to Vestas Wind Systems, Siemens Wind Power, LM Wind Power and DONG Energy for their support.

References

[1] Aeroelastic optimization of mw wind turbines. Technical Report Risø-R-1803(EN), Technical University of Denmark, 2011.

[2] C. Bak and P. Fuglsang. A Method for Deriving 3D Airfoil Characteristics for a Wind Turbine. *AIAA-2004-0666, 42th AIAA Aerospace Sciences Meeting and Exhibit, Reno, NV, USA*, 2004.

[3] C. Bak, J. Johansen, and P.B. Andersen. Three-Dimensional Corrections of Airfoil Characteristics Based on Pressure Distributions. *European Wind Energy Conference, Athens*, 2006.

[4] C. Bak, H.A. Madsen, U.S. Paulsen, M. Gaunaa, N.N. Sø rensen, P. Fuglsang, J. Romblad, N.A. Olesen, P. Enevoldsen, J. Laursen, and L. Jensen. DAN-AERO MW: Comparisons of airfoil characteristics for two airfoils tested in three different wind tunnels. *Torque conference, Crete, Greece*, 2010.

[5] C. Bak, H.A. Madsen, U.S. Paulsen, M. Gaunaa, N.N. Sø rensen, P. Fuglsang, J. Romblad, N.A. Olesen, P. Enevoldsen, J. Laursen, and L. Jensen. DAN AERO MW: Detailed aerodynamic measurements on a full scale MW wind turbine. *EWEC, Warsaw, Poland*, 2010.

[6] P.K. Chaviaropoulos and M.O.L. Hansen. Investigating Three-Dimensional and Rotational Effects on Wind Turbine Blades by Means of a Quasi-3D Navier Stokes Solver. *J. Fluids Engineering*, 122, 2000.

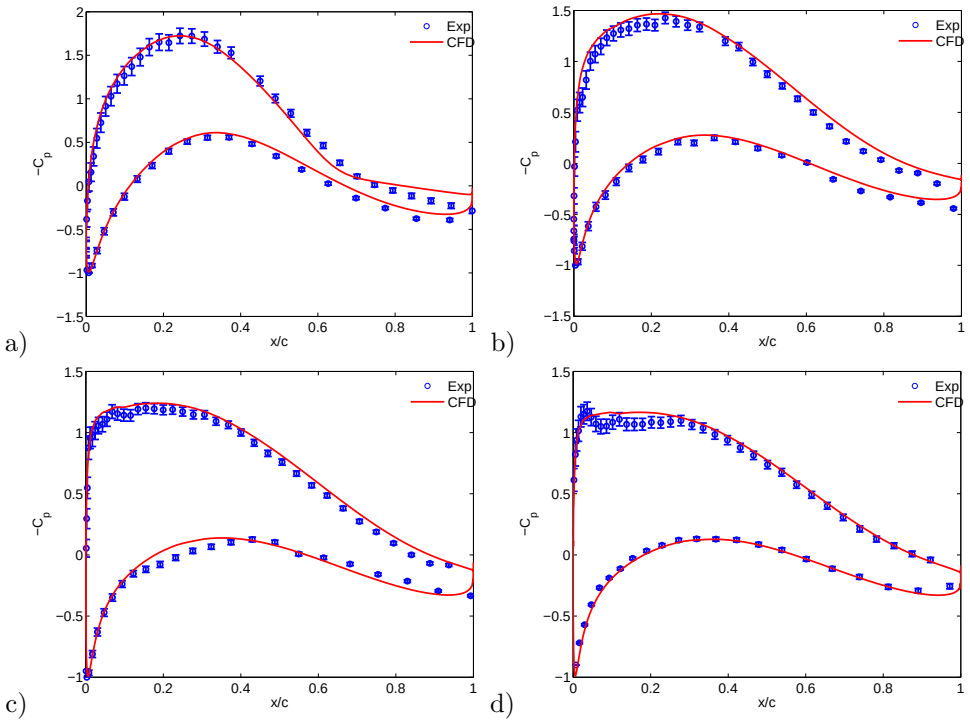

Figure 4: *Comparison of measured and computed C_p distributions on the NM80 turbine operating at $V_\infty = 6.1ms^1$ at a rotational speed of 12.1 RPM and a pitch angle of* 0.15^o. *a) r/R=0.325; b) r/R=0.475; c) r/R=0.750; d) r/R=0.925.*

[7] Z. Du and M.S. Selig. A 3-D Stall-Delay Model for Horizontal Axis Wind Turbine Performance Prediction. *AIAA-98-0021, 36th AIAA Aerospace Sciences Meeting and Exhibit, Reno, NV, USA*, 1998.

[8] P. Fuglsang, I. Antoniou, K.S. Dahl, and H.A. Madsen. Wind tunnel tests of the ffa-w3-241, ffa-w3-301 and naca 63-430 airfoils. Technical Report Risø-R-1041(EN), Technical University of Denmark, 1998.

[9] S. Guntur, C. Bak, and Sørensen N.N. Analysis of 3d stall models for wind turbine blades using data from the mexico experiment. *13th International conference on Wind Engineering, ICWE, Amsterdam, Holland*, 2011.

[10] M. Hand, D. Simms, L. Fingersh, D. Jager, J. Cotrell, S. Schreck, and S. Larwood. Unsteady Aerodynamics Experiment Phase VI: Wind Tunnel Test Configurations and Available Data Campaigns. *NREL/TP-500-29955*, 2001.

[11] J. Johansen and N.N. Sørensen. Airfoil characteristics from 3d cfd rotor computations. *Wind Energy*, 7, 2004.

[12] C. Lindenburg. Modelling of Rotational Augmentation Based on Engineering Considerations and Measurements. *European Wind Energy Conference, London*, 2004.

[13] H.A. Madsen, C. Bak, U.S. Paulsen, M. Gaunaa, N.N. Sø rensen, P. Fuglsang, J. Romblad, N.A. Olesen, P. Enevoldsen, J. Laursen, and L. Jensen. The DAN-AERO MW Experiments. Final report. *Risø-R-1726(EN)*, 2010.

[14] H.A. Madsen, C. Bak, U.S. Paulsen, M. Gaunaa, N.N. Sø rensen, P. Fuglsang, J. Romblad, N.A. Olesen, P. Enevoldsen, J. Laursen, and L. Jensen. The DANAERO MW Experiments. *AIAA 2010-645, 48th AIAA Aerospace Sciences Meeting and Exhibit, Orlando, Florida*, 2010.

[15] H.Aa. Madsen. Aerodynamics of a horizontal-axis wind turbine in natural conditions. *Risø-M-2903*, 1991.

[16] F.R. Menter. Zonal two equation k-ω turbulence models for aerodynamic flows. *AIAA Journal*, (93-2906), 1993.

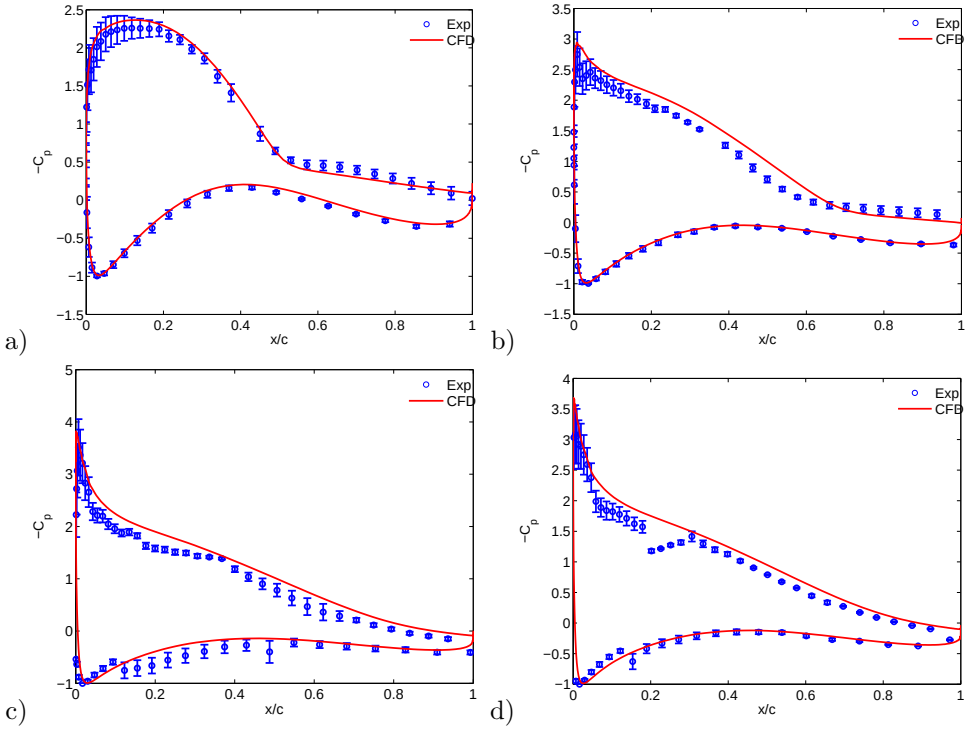

Figure 5: *Comparison of measured and computed C_p distributions on the NM80 turbine operating at $V_\infty = 10.5ms^1$ at a rotational speed of 16.2 RPM and a pitch angle of -4.75^o. a) r/R=0.325; b) r/R=0.475; c) r/R=0.750; d) r/R=0.925.*

[17] F.R. Menter, R.B. Langtry, S.R. Likki, Y.B. Suzen, P.G. Huang, and S. Völker. A correlation-based transition model using local variables, part i - model formulation. *Proc. of ASME Turbo Expo, Power for Land, Sea and Air. Vienna, Austria*, 2004.

[18] F.R. Menter, R.B. Langtry, S.R. Likki, Y.B. Suzen, P.G. Huang, and S. Völker. A correlation-based transition model using local variables, part ii - test cases and industrial applications. *Proc. of ASME Turbo Expo, Power for Land, Sea and Air. Vienna, Austria*, 2004.

[19] J.A. Michelsen. Basis3D - a platform for development of multiblock PDE solvers. Technical report AFM 92-05, Technical University of Denmark, Lyngby, 1992.

[20] J.A. Michelsen. Block structured multigrid solution of 2D and 3D elliptic PDEs. Technical Report AFM 94-06, Technical University of Denmark, 1994.

[21] Hansen M.O.L. and J. Johansen. Tip studies using cfd and computation with tip loss models. *Wind Energy*, 7, 2004.

[22] J.G. Schepers and H. Snel. Model Experiments in Controlled Conditions, Final report. *ECN-E-07-042, Energy Research Center of the Netherlands, ECN*, 2007.

[23] H. Snel, R. Houwink, and G.J.W. van Bussel. Sectional Prediction of 3D Effects for Stalled Flow on Rotating Blades and Comparison with Measurements. *European Community Wind Energy Conference, Lübeck-Travemünde, Germany*, 1993.

[24] N. N. Sø rensen, A. Bechmann, and F. Zahle. 3d cfd computations of transitional flows using des and a correlation based transition model. *Wind Energy*, 14, 2011.

[25] N.N. Sørensen. *General Purpose Flow Solver Applied to Flow over Hills*. PhD thesis, Technical University of Denmark, 1995.

[26] Shen W.Z., Hansen M.O.L., and Sørensen J.N. Determination of the angle of attack on rotor blades. *Wind Energy*, 12, 2009.

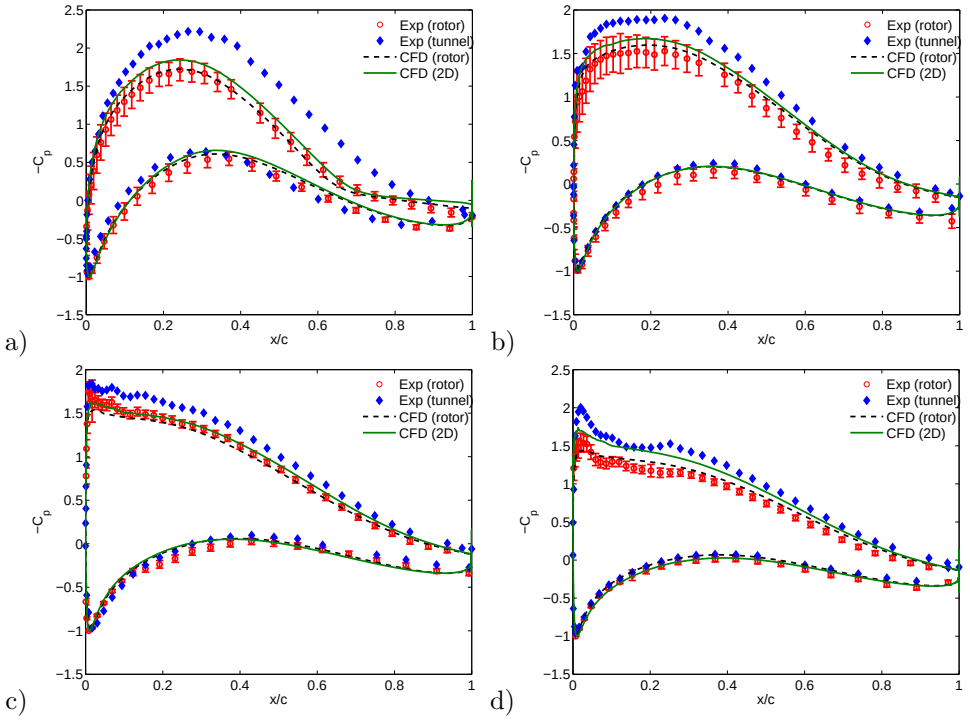

Figure 6: *C_p distributions for the four different blade sections at AoA = 4^o. a) r/R=0.325; b) r/R=0.475; c) r/R=0.750; d) r/R=0.925.*

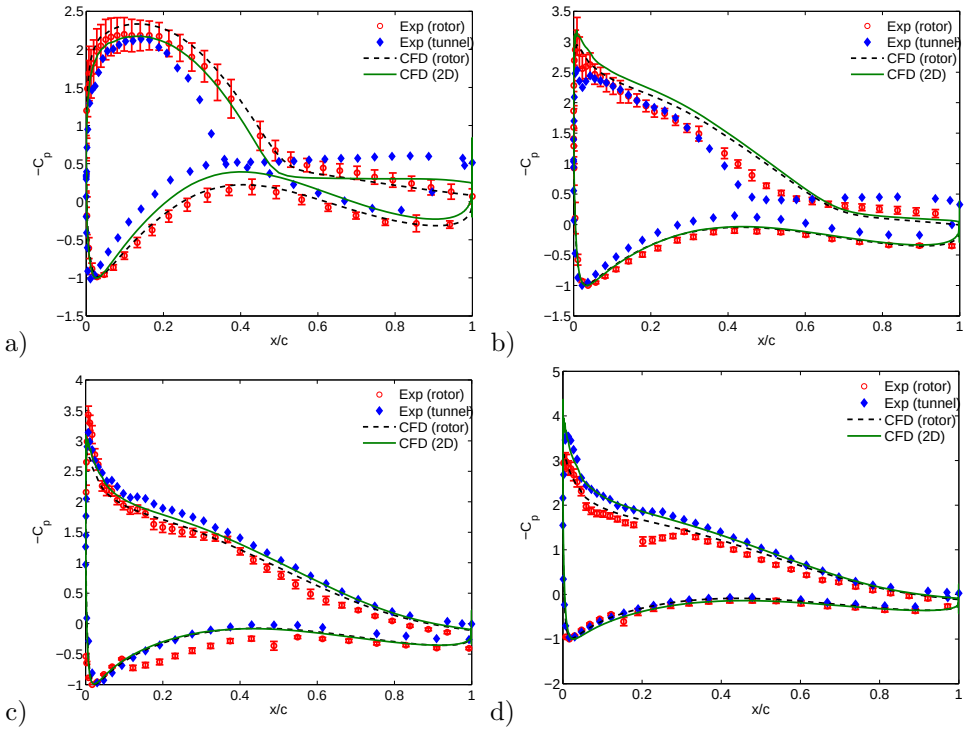

Figure 7: *C_p distributions for the four different blade sections at different AoA. a) r/R=0.325 (AoA = 14^o); b) r/R=0.475 (AoA = 12^o); c) r/R=0.750 (AoA = 9^o); d) r/R=0.925 (AoA = 10^o).*

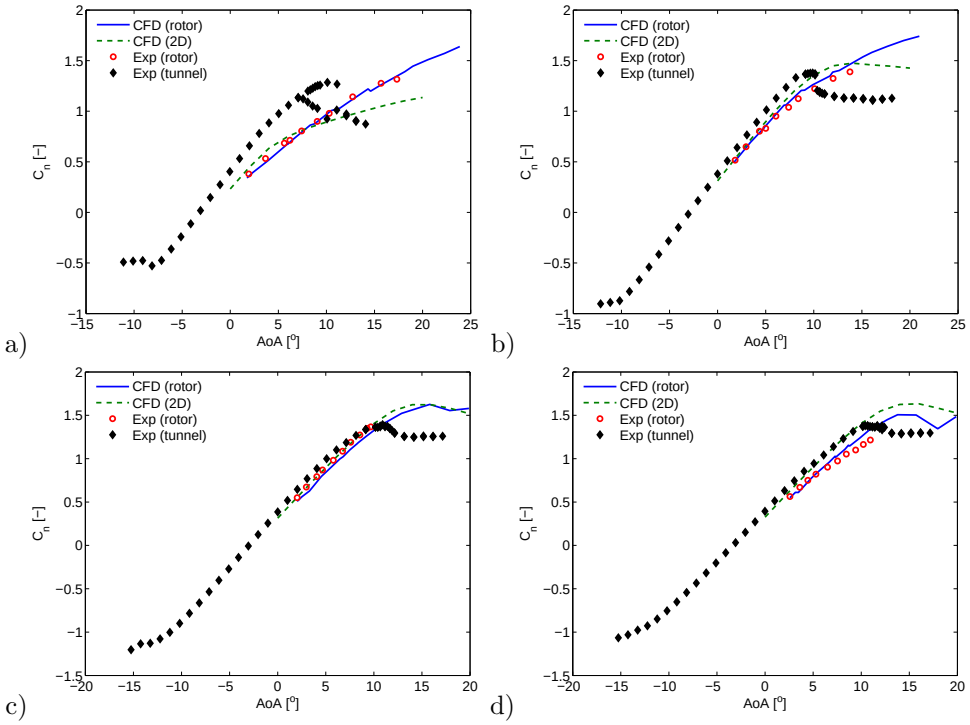

Figure 8: *C_n polars for the four different blade sections. a) r/R=0.325; b) r/R=0.475; c) r/R=0.750; d) r/R=0.925.*

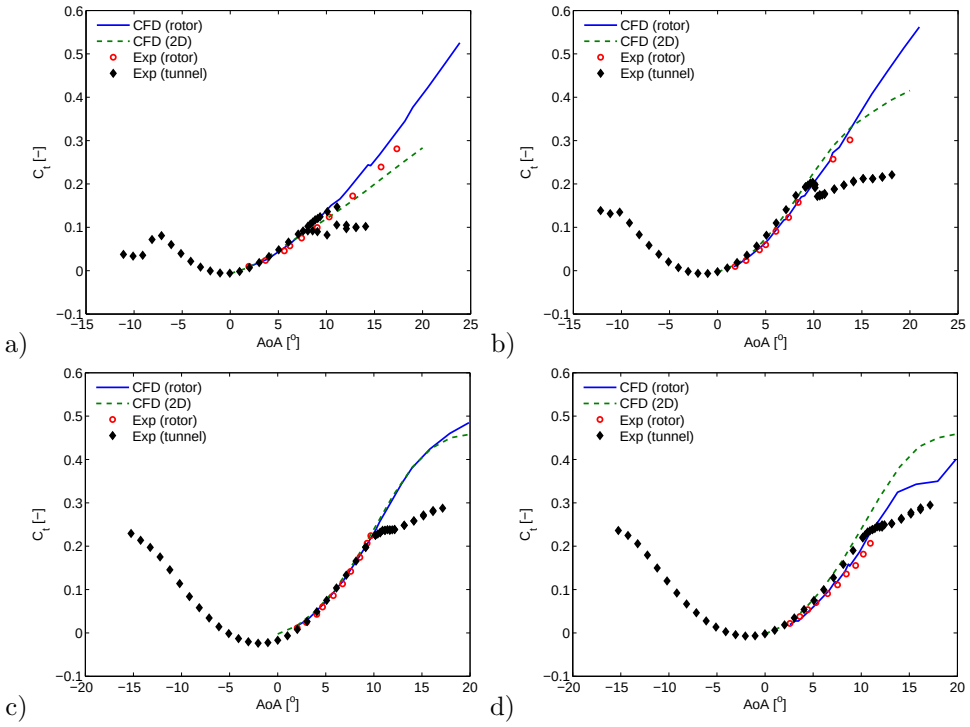

Figure 9: *C_t polars for the four different blade sections. a) r/R=0.325; b) r/R=0.475; c) r/R=0.750; d) r/R=0.925.*